Microsyst Technol (2016) 22:1883–1892
DOI 10.1007/s00542-016-2887-2

TECHNICAL PAPER

Manufacturing of membranes by laser ablation in SiC, sapphire, glass and ceramic for GaN/ferroelectric thin film MEMS and pressure sensors

J. Zehetner[1] · S. Kraus[2] · M. Lucki[2] · G. Vanko[3] · J. Dzuba[3] · T. Lalinsky[3]

Received: 7 August 2015 / Accepted: 18 February 2016 / Published online: 26 March 2016

Abstract AlGaN/GaN-based high electron mobility transistors (HEMTs), Schottky diodes and/or resistors have been presented as sensing devices for mechanical or chemical sensors operating in extreme conditions. Creation of appropriate diaphragms and/or cantilevers out of substrate materials is necessary for further improvement of sensing properties of such MEMS sensors. The sensitivity of the AlGaN/GaN based MEMS pressure sensor can be modified by membrane thickness. In case of SiC as substrate material of the epitaxial AlGaN/GaN heterostructure layers, we applied laser ablation technique for micromachining of the membranes. We were able to verify the feasibility of this process by fabrication of micromechanical membrane structures also in bulk 3C-SiC, borosilicate glass, sapphire and Al_2O_3 ceramic substrates by femtosecond laser (520 nm) ablation. On a 350 µm-thick 4H-SiC substrate we produced an array of 275 µm deep and 1000–3000 µm in diameter blind holes without damaging the 2 µm GaN layer at the back side. Our experiments indicate that pinhole defects in the ablated membranes are affected by ripple structures related to the polarization of the laser. We developed an ablation technique inhibiting the formation of pin holes caused by laser induced periodic surface structures (LIPSS).

✉ J. Zehetner
johann.zehetner@fhv.at

[1] Research Centre for Microtechnology, University of Applied Sciences, Hochschulstrasse 1, 6850 Dornbirn, Austria

[2] Department of Telecommunication Engineering, Faculty of Electrical Engineering, Czech Technical University in Prague, Technicka 2, 16627 Prague 6, Czech Republic

[3] Institute of Electrical Engineering, Slovak Academy of Sciences, Dubravska Cesta 9, 841 04 Bratislava, Slovakia

1 Introduction

This work is motivated by the need for a new material basis for pressure and strain sensors operating at elevated temperatures. For this purpose, the advantage of excellent piezoelectric properties of III-N compounds, especially gallium nitride (GaN)-related heterostructures are attractive. AlGaN/GaN-based electronic devices can be effectively applied as sensing elements in such sensors. Recently, we have introduced an approach whereby the applied external dynamic force (or pressure) causes the change in a piezoelectrically induced charge between the electrodes of a high electron mobility transistor (Vanko et al. 2011). However, the sensors described in (Vanko et al. 2011) were all manufactured on bulk substrate materials (mainly SiC). Only a few published articles mention the possibilities to apply AlGaN/GaN membranes (grown on SiC substrate) as MEMS sensors. Pearton et al. (2004) introduced similar pressure sensors made of a circular membrane of AlGaN/GaN on a SiC substrate. These concepts are based on conductance measurement and/or on nitride film deflection. Usually, the change in the density of the 2-dimensional electron gas (2DEG) confined at the AlGaN/GaN interface as a consequence of the applied strain is presented (Kang et al. 2003, 2004) as the main reason for the change in conductance. In the fabrication process of the proposed MEMS sensors, the key issue is the creation of appropriate diaphragms necessary for the realization of their multi-sensing properties. Conventional reactive ion etching (RIE) method suffers from low etch rates and the complicated masking procedures. We verified the feasibility of the fabrication of micro mechanic structures in bulk SiC substrates with epitaxial AlN/GaN/AlGaN/GaN heterostructures by femtosecond laser ablation at 520 nm wavelength in combination with RIE for pressure sensor applications. On a 4H-SiC

substrate, we produced an array of 250 µm deep and 500 µm diameter blind holes without damaging the adjacent layer of heterostructures. It was shown that 4H-SiC 80 µm thick diaphragms can be fabricated five times faster with laser ablation in comparison to (RIE) (Vanko et al. 2013). We now also investigate ferroelectric thin films as they can be deposited and micro-patterned by a direct UV-lithography method after the ablation process for a specific membrane design (Benkler et al. 2014). The risk to harm or damage the function of thin films can be eliminated by that fabrication procedure. In addition, this offers the opportunity to use alternative materials for sensor substrates like sapphire, ceramic or even glass. However, in order to create thin membranes without RIE, intense leaking of laser radiation from the ablation area has to be minimized by maintaining a smooth ablation surface during the entire ablation process so that backside damage is suppressed. Some ablation-related defects are also affected by the polarization of the laser light. The ripple structure in SiC is oriented perpendicularly to the laser polarization (Tomita et al. 2007) and we believe that ripples to some extent promote the creation of pinholes, which would perforate a thin membrane. We developed an ablation technique strongly inhibiting formation of ripples and pinholes for membranes of higher quality entirely produced by laser ablation in SiC. Ultra short pulsed laser ablation can fabricate diaphragms with a thickness of more than 20 µm in a variety of materials five times faster than RIE.

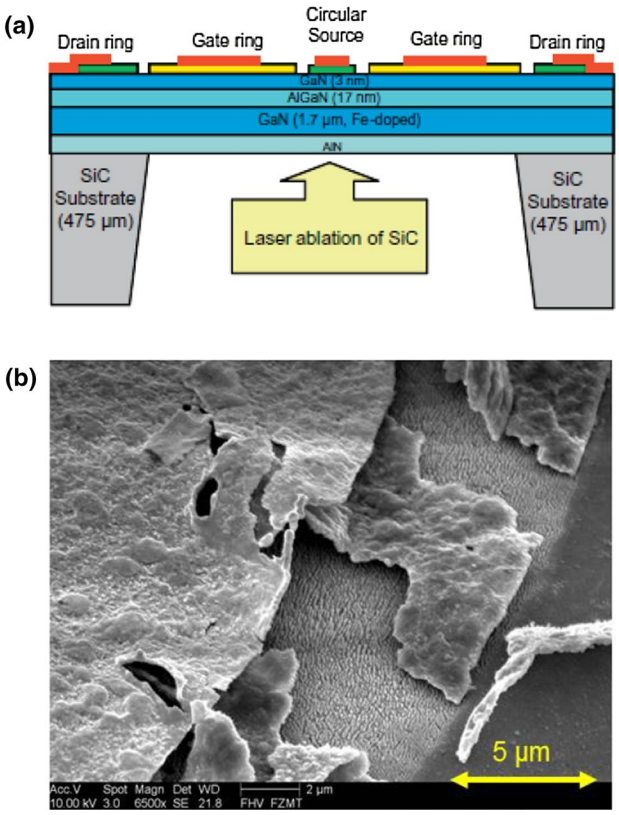

Fig. 1 **a** Detailed cross-section view of the proposed heterostructure layer grown on SiC substrate and **b** SEM micrograph of the damaged metallization after ablation process

2 Device technology and laser ablation processing

2.1 Laser processing system

For experiments we used mainly the ultrafast laser "Spirit" from Spectra-Physics Rankweil, delivering an average power of 4.0 W at 1040 nm and 200 kHz repetition rate with a pulse length of 380 fs; the system delivers also second harmonic (SH) at 520 nm, where we get about 1.5 W at 100 mm focal length of the telecentric scanner optics. The maximum pulse energy was $E = 10$ µJ and the focus radius was $w_0 = 6$ µm. The Spirit was integrated in a laser processing machine (3D-Micromac, microSTRUCT vario).

The laser beam was linearly polarized and in some experiments, the direction of the polarization was altered by 90° during scanning or the sample was rotated.

2.2 Sensor design and technology

The heterostructures for the transistor processing technology were grown on a 350 µm thick 4H-SiC substrate using a proprietary nucleation layer. It consists of a 1.7 µm thick Fe-doped GaN buffer followed by an unintentionally doped 17 nm thin AlGaN (with a 29.5 % Al mole fraction) barrier and a thin, 3 nm GaN cap epitaxial layer shown in Fig. 1a. The proposed sensing devices utilize the piezoelectric properties of the active AlGaN barrier layer and are formed by two different types of metallization schemes, which act as the sensing (charge collecting) electrodes. First, the ohmic contacts of the C-HEMTs (circular-high electron mobility transistors) using an Nb/Ti/Al/Ni/Au metallization scheme were deposited by electron beam and thermal evaporation techniques and annealed at 850 °C for 35 s. As a second step, metallization based on Ni/Au layers was employed as the Schottky gate electrode. Finally, Ti/Au metallic layers are patterned on the top of the alloyed ohmic and Schottky contact metallization layers to improve the device bonding and interconnection.

Piezoelectric polarization in the AlGaN/GaN heterostructure layer can be changed by an external action. This means that a change in the density of the (2DEG), located at the AlGaN/GaN interface, takes place. As a result, the HEMT conductivity can be influenced by external strain. Thus HEMTs based on AlGaN/GaN heterostructures have appeared to be excellent candidates for pressure sensing (Kang et al. 2003, 2004). The piezoelectric response

to external mechanical loading was investigated and verified. Functionality of the proposed circular diaphragms was evaluated at room temperature and low static and dynamic pressure loading (Dzuba et al. 2015).

Backside damage of the material structure during the ablation process was a serious threat for membrane ablation. Within ten consecutive scans the metallized backside of the sensor device was usually destroyed as can be seen in the picture in Fig. 1b. However, on average we required about 1000 scans to obtain the desired depth for membrane fabrication and that forced us to change the manufacturing procedure. We used a plain substrate with the epitaxial grown functional layer only and the first technological step was the laser ablation as close as possible to the backside (exit side of the laser beam after ablation on front side) in order to produce thin membranes or to reduce the material thickness to be removed in case a subsequent RIE process is required (than masking was the first step). Whatever case it is essential that the ablated surface remains flat and straight for every single laser ablation scan as any tiny obstacle created on the ablated surface will couple light towards the backside where it can cause damage. In particular, 3C-SiC was very sensitive against pinhole formation and backside damage, as can be seen in Fig. 2 the pictures on the right side. Backside damage was also a threat for 4H-SiC coated with the AlGaN/GaN heterostructure layer but pinhole formation was much easier to control due to the bigger laser parameter window. A reason for that effect might be the higher purity and quality of the 4H-SiC substrate. As for a backup technology should a required membrane thickness be out of reach with the epitaxial layer on the back side of SiC, we started to investigate lead strontium titanate thin PST ($Pb_{0.4}Sr_{0.6}TiO_3$) film systems on sapphire, ceramic and glass. These films can be applied after laser ablation and the risk for backside damage is reduced. The PST films were manufactured using a polymer-based deposition and patterning direct UV-lithographic process. We reported this process in detail in a publication (Benkler et al. 2014). Due to the simple sol synthesis and the straightforward process, this method is an interesting alternative to other deposition and patterning processes. For these reasons, this process was used to manufacture micro-patterned ferroelectric films on top of the membranes produced by laser ablation. An additional advantage is that there is no need to use a specific substrate material for crystal lattice matching with the functional membrane layer.

2.3 Thin membrane fabrication by laser ablation

We present procedures and results for the fabrication of diaphragms with various thicknesses and diameters in bulk sapphire, Al_2O_3-ceramic, borosilicate glass and SiC with epitaxial AlN/GaN/AlGaN heterostructure layers. Some

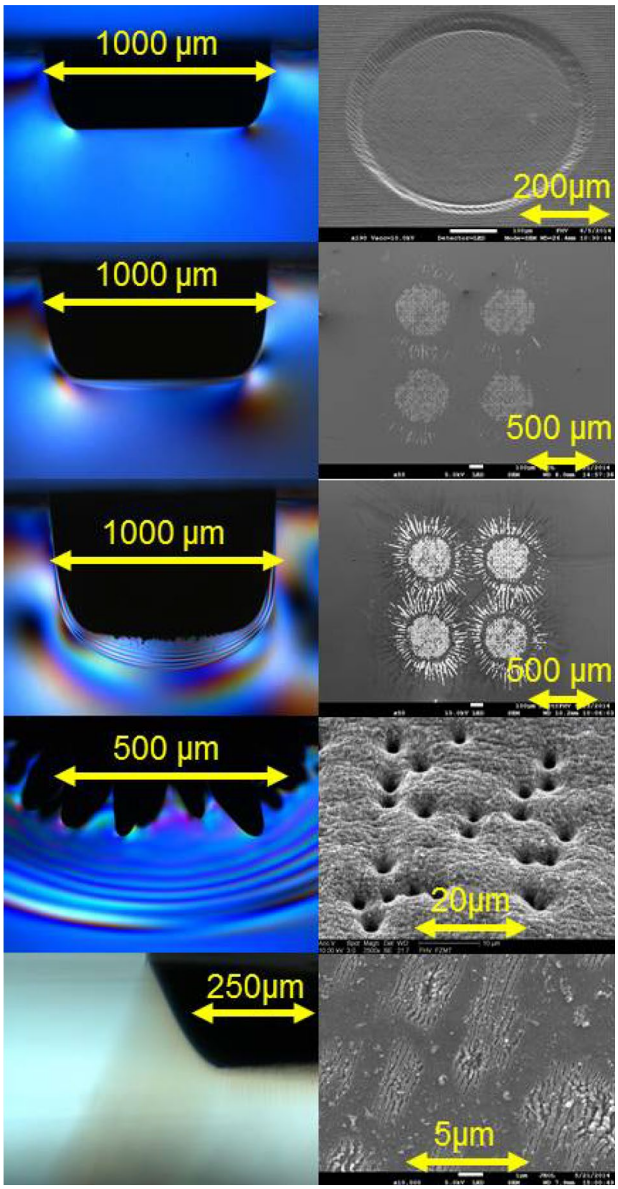

Fig. 2 *Left picture* column, growing surface roughness with increasing ablation depth in PC, *left bottom picture* show *color* centers in glass indicating the radiation loss. *Right picture* column, shows corresponding backside damage and pinhole formation all in SiC as a consequence of the leaking radiation. The *upper* and the *fourth picture* show the *bottom* of a bore from the *front-side*

possible damage mechanism and its cause in the process of fs-ablation are qualitatively analysed, summarized and visualised in Fig. 2. Due to the complex interaction of various laser parameters it is very helpful to get a general view and understanding to target effectively the parameter and process optimization in the ablation procedure. In our optimized laser ablation procedure, the membrane quality did not deteriorate from pinhole formation, and backside damage.

We used polycarbonate (PC) and glass to visualize critical geometries, cause and consequences from leaking

laser radiation hitting the back side of the sample. In PC, we ablated cavities with different depth and laser radiation penetrating into the bulk generated birefringence, in glass induced color-centers made leaking laser light visible as a shade emerging from the side wall of the bore (Fig. 2 left undermost picture). In five different PC sample cross sections the growing surface roughness during the ablation progression becomes viewable (Fig. 2 left pictures) and the consequence of increased coupling of laser radiation into the bulk via pinholes is demonstrated. Starting with a shallow bore at the top of Fig. 2, the ablation area shows uniform surface quality all over; only the corners indicate radiation loss to the bulk. Deeper bores produced by bigger numbers of scans show an increase of surface roughness, pinhole formation and general quality deteriorates at the bottom of the bore as well at the side wall. Using a polarization microscope one can visualize the radiation dose-related birefringence (bluish pictures on the left); the dose coupled into the bulk is growing in the pictures at the left side of Fig. 2 from the first shallow bore at the top to the forth deepest bore which shows an enlarged detail section at the bottom with heavy pinhole formation. The progression of laser scanning increases surface roughness and promotes finally pinhole formation. As a consequence, a higher part of the laser light is not utilized for ablation but launched deep into the material where it heats up the bulk and causes strain and birefringence as well as damage on the back side of the sample. Our investigations in (Zehetner et al. 2015) revealed that this problem of pinhole formation is severe mainly in 3C-SiC and places less stringent limitations in 4H-SiC. The last row of pictures in Fig. 2 shows the leakage of radiation from the sidewall of the bore in the cross section of a glass sample (left picture undermost row) and the corresponding damage (right picture undermost row) at the back side of a 3C-SiC sample. The pictures in the second and third row of the right column in Fig. 2 show the corona like damage at the back side in 3C-SiC. The corona is asymmetric due to the Brewster effect and related to the losses from the side wall, the round center damage is caused by direct laser light transmission through the bottom.

Above observations imply that leaking of laser light from the ablation area has to be minimized by maintaining a smooth pattern surface during the entire ablation process in order to suppress the backside damage. We realized that small pinholes are first formed in the corner of the bore in the direction perpendicular to the polarization direction. Later they can appear all over the surface. Laser light is coupled very effectively to the back side of the sample via these pinholes causing heavy surface damage. There are no or at least a very few such small holes in the polarization direction and we made the observation that pinholes are formed primarily in metals and semiconductors, when laser-induced periodic surface structures (LIPSS) are at some positions disrupted by scratches, particles or a side wall. The mechanism of such pinhole formation in SiC is yet not completely clear. Our hypothesis to explain the spatial relation between LIPSS, scratches and pinholes in SiC is the high refractive index and the small dimension of the LIPSS (100–800 nm period with about 50–200 nm slots in between). The assumption is that LIPSS in SiC might serve as slot waveguides, scratches, other obstacles or a bore wall can lead to field enhancement. We generated also LIPSS on steel scratched samples and predominately on locations where scratches on the surface crossed and disrupted the LIPSS we observed strong pinhole formation, equal results were reported in research on the influence of the surface finish on the generation of LIPPS (Preutsch et al. 2015; Hou et al. 2011). This slot waveguide approach is additionally supported by the fact that we had no problem with pinholes in material with lower refractive index like sapphire, Al_2O_3-ceramic or glass; although LIPSS are formed they would not function as slot waveguides. We observed them mainly in SiC, Si and metals. We did some simulations on slot waveguides and the results showed increased field intensity at the beginning of the slot and this is in agreement with the mentioned observations. However, to rule out that pinhole formation is not highly influenced by the scanning mode (xy-grid, rotating xy-grid, arbitrary direction, or rotating sample), focus position or laser power we did some further experiments.

In the first experiments, the focus was set on top of the sample with about 400 µm thickness (upper row of Fig. 3) in the middle (middle row) and on the bottom (bottom row). In all three cases the laser power was 350 mW and resulted in an ablation depth of approximately 200 µm for all three focus positions. The final ablated surface position when the focus was set in the middle of the sample was than exactly in the focus plane. We used a xy scanning pattern with 5 µm hatch. This pattern was graphically rotated in 15° increments after one finished scan (sample position was fixed) and at every increment the polarization was in the left to right x direction (parallel to the 0° starting direction of the x-axis of the rotating scan grid). The results of the surface quality are shown in the right column of Fig. 3. Only the test with the focus position in the middle of the sample developed damage on the membrane in an area close to the bore wall perpendicular to the polarization direction (indicated by red arrows and an enlarged picture of this position is shown in Fig. 5). LIPSS are also orientated perpendicular to the linear polarized laser light and the damage is generated in an area were the LIPSS (slot waveguides) are disturbed and blocked by the side wall of the bore. No pinholes have been observed on the rest of the membrane. The depth of the bore is close to 200 µm; that means the laser fluence at the finished

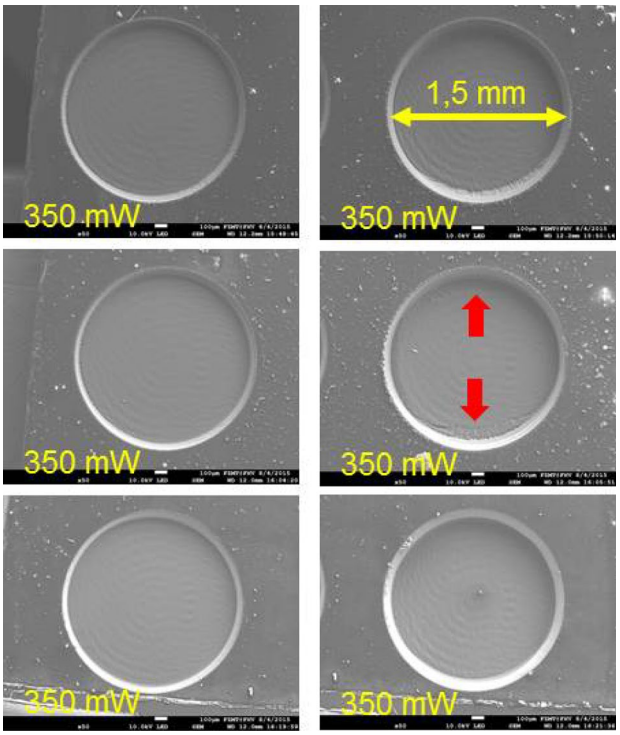

Fig. 3 Parameters on test are polarization and focus position. *Left* colomn represents the results with flipped polarization between x- and y-axis, *right* column shows fixed polarization along x-axis. Focus position on *upper sample* surface (*top picture row*), in the *middle of sample* (*middle pictures*) and the *sample bottom* (*bottom picture row*)

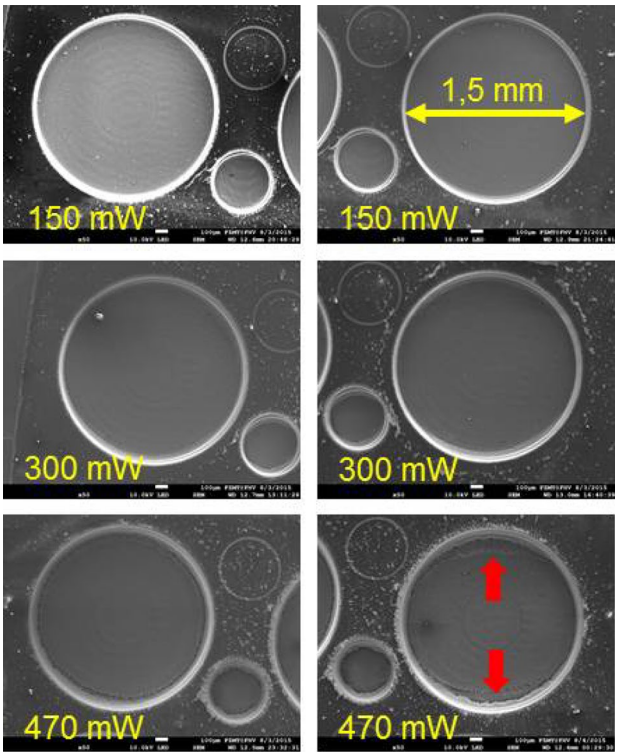

Fig. 4 The parameters on test are laser power and polarization. Focus position is fixed in the *middle of the sample*. *Left picture* column represents results with flipped x-, y-polarization, *right* column gives results with fixed polarization in x-direction

membrane surface is higher (approximately in the focus plane) with respect to the two other test positions, which are both about 200 µm out of focus plane. It means that the quality influencing parameter is not the focus position but the laser power or fluence on the surface of the finished membrane. In addition, in case the LIPSS are involved in the surface damage formation, the quality should be improved for the focus position in the middle of the sample when the linearly polarized light is in rotation or flipping from x to y direction during the scanning procedure. As the LIPSS are generated perpendicular to the linearly polarized laser, changing direction would destroy continuously the LIPSS from the preceding scan and hence pinholes have no time to grow to a bigger size, they will stay at nanometer dimensions. This was exactly what we observed. Figure 3 left column shows the results from the xy-flipping polarization. The quality in the middle picture row shows significant improvement of the surface and there is no visible damage in the area close to the bore wall (better evidence is shown in the enlarged picture in Fig. 5). The upper and bottom rows have about the same quality, as the fluence to generate pinholes was not obtained at any position in the out of the focus plane. To be sure that the fluence and the polarization are the critical parameters for pinhole formation, we set up an additional test; the results are given in Fig. 4.

In all the experiments shown in Fig. 4, the focus plane was fixed in the middle of the sample. One test series was made again with a rotating scanning pattern at 15° increments and a constant polarization orientation in x-direction (right column Fig. 4). The reference test was made with additional polarization flipping from x- to y-orientation back and forward during the ablation procedure, results are given in the left column Fig. 4). We used here different laser power settings beginning with 150, 300, and 470 mW. The maximum power setting is 120 mW increased with respect to the 350 mW in the previous experiments. In case there is a threshold for the pinhole formation, the damage at fixed polarization orientation should be more distinctive and the pinholes spread over a bigger area on the membrane. Reduction of damage with respect to the test at fixed polarization orientated in x-direction and inhibited pinhole formation in the test with changing polarization direction would again strongly indicate that LIPSS are heavily involved in pinhole formation in SiC membranes. The obtained results were accordingly to our expectations. Up to a laser power of 300 mW the surface quality of the membranes is similar at fixed polarization (Fig. 4 right column)

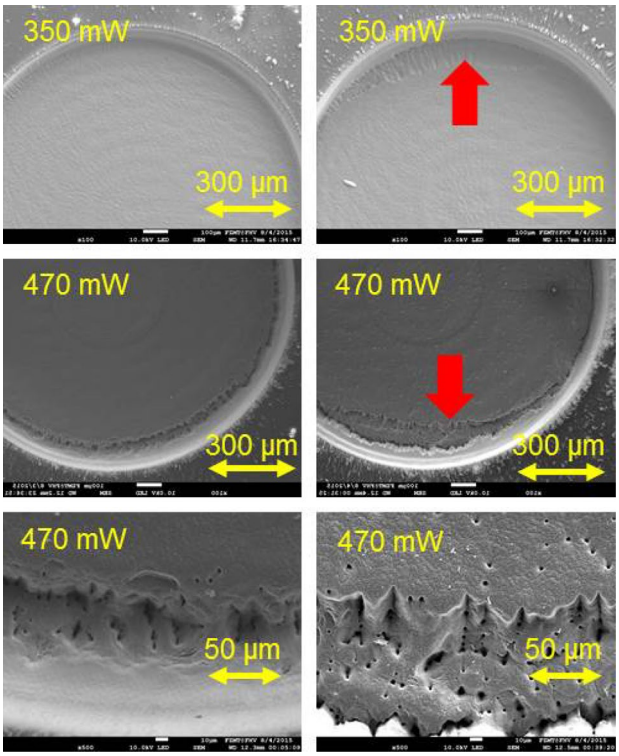

Fig. 5 Results in 3C-SiC for a xy-scanning pattern rotating at 15° increments, at fixed polarization in x-direction (*right picture column*), slight damage in the *arrow* marked corner area at 350 mW without pinholes in the membrane (*upper picture*), heavy damage at 470 mW in at the *arrow* marked position and pinholes all over the membrane (*middle and lower picture*). Damage reduction by flipped polarization at same laser parameter (*left column*), at any laser power reduced damage in the corner area and no pinholes in the membrane

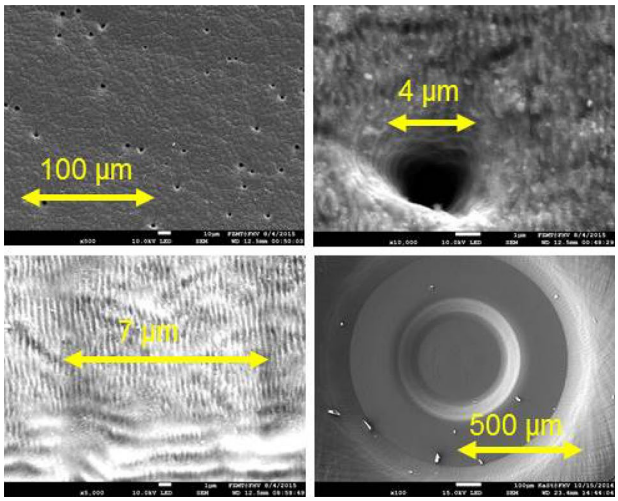

Fig. 6 All pictures are from 3C-SiC samples. *Upper left* picture shows pinholes in the center area of the membrane. *Upper right* picture depicts a single pinhole surrounded by LIPSS. *Lower left* picture shows the corner area and LIPSS in a bore short time before pinhole formation. *Lower right* picture gives the results with a rotating sample LIPSS, pinholes and corner distortion can be suppressed

and changing polarization direction (Fig. 4 left column). No pinholes were observed on the membrane and only little damage in the region close to the wall of the bore. At changing polarization condition, the results were only slightly better. Increase of the power to 470 mW caused heavy damage at fixed polarization mainly perpendicular to the orientation of the polarization (red arrow mark). The generated LIPSS are in there orientation pointing towards this damage region supporting our slot waveguide hypothesis (more enlarged pictures depict the LIPSS in Fig. 6). At fixed polarization and 470 mW, pinholes occurred all over the membrane, they are only 3–5 µm in diameter and the lower right picture in Fig. 5 shows them enlarged together with the damage area close to the bore wall. The upper right picture in Fig. 5 shows the center area as well as a slightly damaged area close to the wall of the bore (indicated by red arrows) with a fixed polarization in x-direction at 350 mW and the picture in the middle at 470 mW of laser power. There are no pinholes in the center area of the membrane at 350 mW ablation power that means there is threshold fluence for pinhole formation. Changing polarization during ablation even at 470 mW laser power leads to a significant reduction of the damage in the corner area of the bore and eliminates the formation of the pinholes on the membrane (Fig. 4 left bottom picture and Fig. 5 left pictures in the middle and bottom row enlarged). We can conclude that pinhole formation has a higher threshold when the polarization direction is permanently changed after each scan and that LIPSS are very much involved in the process of pinhole formation. The parameter window for the laser power can be increased by permanently changing the orientation of the polarization which improves quality and stability of the ablation process, this is very important for the fabrication of thin membranes. LIPSS on SiC are formed perpendicular to the polarization direction at the very first scan but will be disordered in a single subsequent scan at altered polarization direction. However, according to our experiments pinholes require several scans to grow and consequently polarization flipping contributes effective to avoid them. In addition, we observed that formation of pinholes starts more likely when LIPSS are interrupted by obstacles, scratches or particles from debris on the membrane. When LIPSS are reorganized in a new direction at sufficient short time these obstacles move out of function and the pinholes cannot continue to grow. This supports also our assumption that on high refractive index material LIPSS act as a slot waveguide. First simulations indicate the same conclusion.

At 470 mW ablation power pinholes evolved all over the membrane not only in the corner area. Figure 6 upper left picture gives an impression from the pinhole distribution in the center area of the membrane. Further increase of

power or number of scans would also increase the number of pinholes. The upper right picture shows a single pinhole, the diameter is typically in the range of 3–5 µm. Laser light entering such a hole is trapped and guided into the bulk of the SiC sample and finally to the backside. This can cause backside damage of the sample itself or on applied surface coatings. Beside that a perforated membrane is not acceptable. At lower ablation power, the pinholes are not created all over the membrane the formation starts first in the corners of the bore. Edges and rims of the sidewall can lead to interfering patterns close to the corners at the bottom of the bore and if intense enough wavelike structures are formed (not to be confused with LIPSS in this case formed with 500 nm periodicity parallel to y-direction). One can see such a structure parallel to the x-direction in the lower left picture of Fig. 6. The increment between these interference ripples was slightly more than 1 µm. Two further groves can be seen parallel to the y-direction about 7 µm apart. In the zone where interference ripples and LIPSS start to interact we predominately observed the first pinholes. The formation of such interference ripples and LIPSS was very effective suppressed when the sample was rotated with about 30 rpm during ablation leading to a very smooth result as can be seen in Fig. 6 lower right picture.

The disadvantage of such an approach is that one con produce only one single circular structure. Different shapes or a pattern array need a more practical method. We could demonstrate that much simpler polarization switching in combination with rotation of the scanning direction (not the scanned pattern itself) provides a wider parameter window sufficient to suppress pinhole formation in membranes.

Membranes laser ablated in sapphire and glass got no pinholes and we achieved a smooth surface, as can be seen in Fig. 7 upper picture row; the right-hand picture shows a cross section in glass. Sapphire and glass have a much lower refractive index compared to SiC and LIPSS do not have such slot waveguide characteristic as in SiC. For 4H-SiC, we could find good ablation parameter far below the threshold for pinhole formation. However, rotating the sample improved also the membrane quality significant as shown in Fig. 7 bottom picture row; the right picture represents the result for the rotating sample.

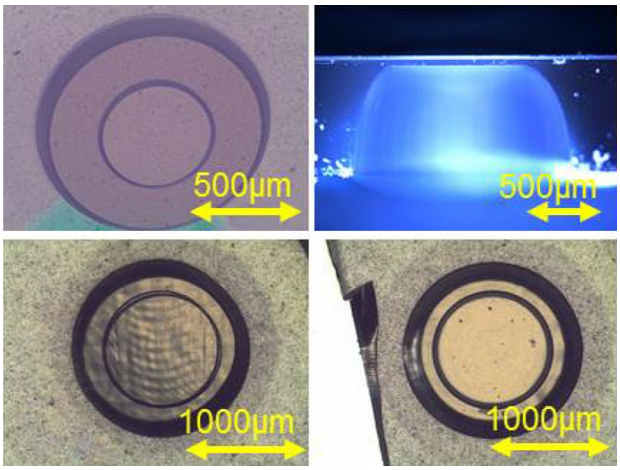

Fig. 7 In sapphire glass and ceramic, there was no pinhole formation observed, *left upper picture* shows a membrane in sapphire, *right upper picture* a cross section of a 50 µm membrane in glass. 4H-SiC has a high threshold for pinhole formation, *bottom picture row*, but rotating the sample improves membrane quality as shown in the *bottom right picture*

3 Numerical LIPPS waveguide structure simulation

We performed a numerical study of light propagation and its interaction with selected shapes of grooves acting as a waveguide in SiC material. The simulations are achieved using the finite difference time domain (FDTD) method (Taflove et al. 2005), which is suitable for this purpose, since it allows calculating both time-evolution and spectrum of an electromagnetic field. The studied structure is formed by grooves inscribed by a laser into SiC. The grooves on the surface of SiC resemble either prisms with oblique side-walls or rectangles (Fig. 8). Two distinct geometrical arrangements of the grooves are considered in the simulations. The first arrangement in a form of an array layout is depicted in Fig. 8 (top), where grooves are longitudinally oriented in series. In another arrangement, Fig. 8 (the middle picture), the grooves are placed zig-zag along y-axis, such that their longitudinal axes overlap with the center of gap between the grooves in the adjacent column.

In Fig. 8, the dash-dotted line indicates YZ plane cut at x = 0.5 µm and the cross-section of the array layout structure is presented, with y-polarized laser source and propagation of light along z-axis (z = 0 is at surface). The groove width and depth are labeled as w and d, respectively Table 1. Longitudinal gap between columns of grooves is shown as g, transversal gap as a, and period as Λ. The values of all geometrical parameters considered in the simulations are summarized in The model of a laser source produces a Gaussian beam with focus radius $w_0 = 10$ µm. Optical pulses with the output spectrum centered at 1040 nm are launched from a plane parallel to the surface of SiC and propagated along z axis—Fig. 8, bottom picture. Polarization of the source is set along y-axis. Material properties of SiC (type 6H α-SiC) are modeled using polynomial approximation of the published experimental data (Hofmeister et al. 2009). Since the dimensions of the structure greatly vary, it is crucial to utilize non-linear mesh near the surface along with conformal meshing technique (Yu and Mittra 2001) to accurately resolve sub-cell features of the structure.

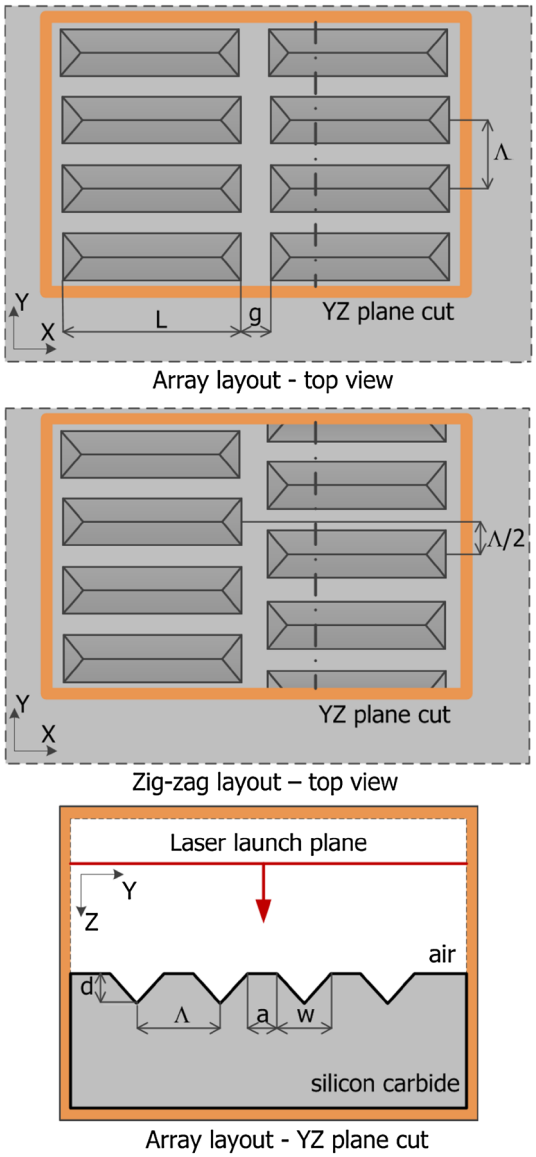

Fig. 8 Side-cut of the studied structure with structural parameters and simulation boundaries

Tab.1 Structural parameters of the investigated structure

Groove length *L*	3 μm
Longitudinal gap *g*	200 nm
Periodicity *Λ*	500 nm
Width of surface gaps *a*	200 nm
Groove width *w*	300 nm
Groove depth *d*	50 or 100 nm

From Figs. 9, 10, 11, and 12, it can be concluded that light intensity is in good agreement with the places, where pinholes in SiC are formed. The simulation showed that

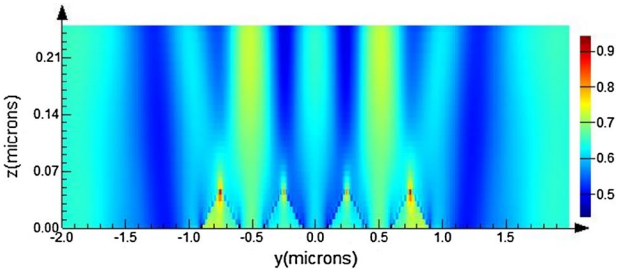

Fig. 9 Field intensity profile in YZ plane cut at x = 0.5 μm for depth of grooves d = 50 nm

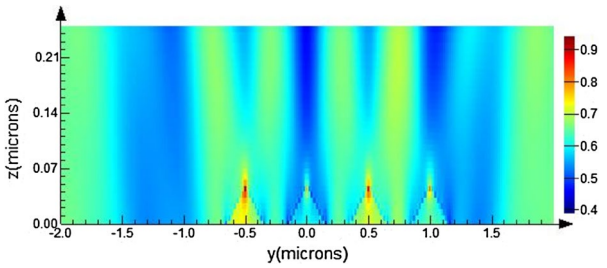

Fig. 10 Field intensity profile in YZ plane cut at x = 0.5 μm. Grooves are aligned in alternating arrangement (*zigzag*) with depth of grooves d = 50 nm

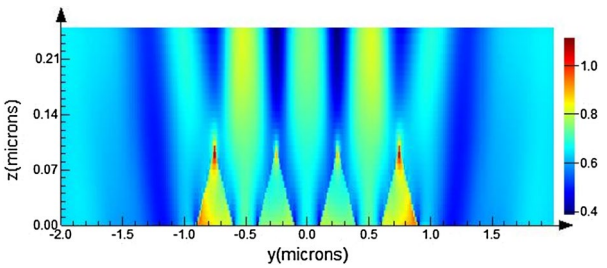

Fig. 11 Field intensity profile in YZ plane cut at x = 0.5 μm for depth of grooves *d* = 100 nm

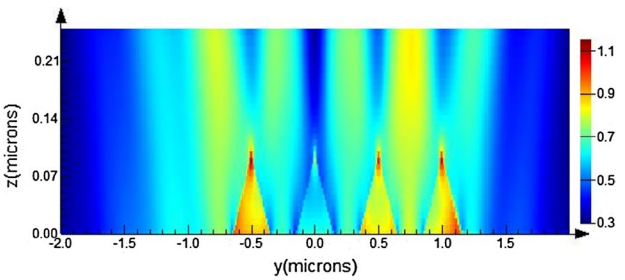

Fig. 12 Field intensity profile in YZ plane cut at x = 0.5 μm. Grooves are aligned in alternating arrangement (*zigzag*) with depth of grooves d = 100 nm

field intensity is enhanced in a certain small depth (see results compared for the depth of 50 and 100 nm), which could explain the formation of pinholes just at the scratch location, in the corners. Moreover, different orientation of the grooves influences the amount of light transmission into SiC. Considering the arrangement of grooves oriented along x-axis and light propagation along z-axis, results for different intensity values for both polarizations, were also verified by changing the orientation of the grooves. It means strong influence of incident light polarization on transmission characteristics. This would explain why polarization rotation stops pinhole formation. The LIPSS are generated perpendicular to the polarization of light. When the polarization is changing LIPPS are changing direction and pinholes have no time to establish.

4 Conclusion

Using femtosecond laser ablation, we manufactured 150 µm thin membranes in 3C-SiC as well 80 µm membranes in 4H-SiC and verified the feasibility of a rotating polarization process to suppress sub-µm ripple and pinholes in micro machined structures. For sensor test application, we used our standard ablation xy-scanning procedure and fabricated arrays of membranes in 4H-SiC (115 µm), Pyrex glass (40–80 µm), sapphire (50 and 160 µm) and in Al_2O_3 ceramic (25–90 µm). The various membranes are 1000, 1500, 2000, and 3000 µm in diameter. The back side of the 4H-SiC was covered with an epitaxial grown 2 µm AlN/GaN/AlGaN layer and was not damaged after ablation. Substrates of all other materials investigated were plain and were coated with ferroelectric thin films after the ablation process. The risk to harm or damage the function of the coated films is eliminated by that procedure and a higher degree of freedom for design is achieved.

Our experimental results and first simulations indicate that ripples promote creation of pin holes in SiC, which would perforate a thin membrane in a sensor (Fig. 1). We developed an ablation technique strongly inhibiting formation of ripples and pin holes (Fig. 2) for higher quality membranes entirely produced by laser ablation. In our technique, the direction of the linearly polarized light rotates permanently or is flipped between x- and y-axis and as a consequence ripples could not be generated for a time period long enough to enable pinholes to begin to form and grow to µm size. Without changing direction of the polarization, the corners or scratches at the bottom of the blind bores are in exposed position for creation of pinholes with a quite small parameter window to avoid them. The z-position range of the laser focus and the maximum possible laser power increases significantly when the polarization changes during ablation reducing the ablation time and improving the process stability.

Acknowledgments Open access funding provided by FH Vorarlberg - University of Applied Sciences. This work was supported in part by: The Slovak–Austrian bilateral project SK-AT-0019-10, ICM OeAD SK05/2011, Slovak Research and Development Agency under contract APVV0455-12. The CTU Grant under project SGS13/201OHK3/3T/13.

References

Benkler M, Hobmaier J, Gleissner U, Hertkorn D, Medesi A, Hanemann T (2014) Polymer based route to ferroelectric lead strontium titanate thin films. J Appl Polym Sci. doi:10.1002/app.40901

Dzuba J, Vanko G, Držík M, Rýger I, Vallo M, Kutiš V, Haško D, Choleva P, Lalinský T (2015) Stress investigation of the AlGaN/GaN micromachined circular diaphragms of a pressure sensor. J Micromech Microeng 25:015001

Hofmeister AM, Pitman KM, Goncharov AF, Speck AK (2009) Optical constants of silicon carbide for astrophysical applications. II. Extending optical functions from infrared to ultraviolet using single-crystal absorption spectra. Astrophys J 696(2):1502–1516

Hou S, Hou Y, Xiong P, Zhang Y, Zhang S, Jia T, Sun Z, Qiu J, Xu Z (2011) Formation of long and short periodic nanoripples on stainless steel irradiated by femtosecond laser pulses. J Phys D: Appl Phys 44:505401

Kang BS, Kim S, Kim J, Ren F, Baik K, Pearton SJ, Gila BP, Abernathy CR, Pan C-C, Chen G-T, Chyi J-I, Chandrasekaran V, Sheplak M, Nishida T, Chu SNG (2003) Effect of external strain on the conductivity of AlGaN/GaN high-electron-mobility transistors. Appl Phys Lett 83:4845

Kang BS, Kim S, Ren F, Johnson JW, Therrien RJ, Rajagopal P, Roberts JC, Piner EL, Linthicum KJ, Chu SNG, Baik K, Gila BP, Abernathy CR, Pearton SJ (2004) Pressure-induced changes in the conductivity of AlGaN/GaN high-electron mobility-transistor membranes. Appl Phys Lett 85:2962

Pearton SJ, Kang BS, Kim S, Ren F, Gila BP, Abernathy CR, Lin L, Chu SNG (2004) GaN-based diodes and transistors for chemical, gas, biological, and pressure sensing. J Phys: Condens Matter 16:961–994

Preutsch, F., Rung, S., Hellmann, R. (2015) Influence of surface finish on the generation of LIPSS. In: Proceedings of LAMP2015, Kitakyushu

Taflove, A. and Hagness, S. C. (2005) Computational Electrodynamics: The Finite-Difference Time-Domain Method. Norwood: Artech House. Third edition. ISBN 1-58053-8320

Tomita T, Kinoshita K, Matsuo S, Hashimoto S (2007) Effect of surface roughening on femtosecond laser-induced ripple structures. Appl Phys Let 90:153115

Vanko G, Držík M, Vallo M, Lalinský T, Kutiš V, Stančík S, Rýger I, Benčurová A (2011) AlGaN/GaN C-HEMT structures for dynamic stress detection. Sens Actuators Phys 172:98–102

Vanko G, Hudek P, Zehetner J, Dzuba J, Choleva P, Kutiš V, Vallo M, Rýger I, Lalinský T (2013) Bulk micromachining of SiC substrate for MEMS sensor applications. Microelectron Eng 110:260–264

Yu W, Mittra R (2001) A conformal finite difference time domain technique for modeling curved dielectric surface. IEEE Microwave Wirel Compon Lett 11(1):25–27

Zehetner, J., Vanko, G., Dzuba, J., Benkler, M., Lucki, M., Rýger, I., Lalinský, T. (2015) Laser ablation for membrane processing of AlGaN/GaN- and microstructured ferroelectric thin film MEMS and SiC pressure sensors for extreme conditions"MICROTECHNOLOGIES, Barcelona